Article 27: Experimental Facilities and Measurements – Fundamentals

Abstract: Fundamental details of the spatial and/or temporal evolution of in-cylinder processes of internal combustion engines may be gained from various optical diagnostics. Application of optical diagnostics requires experimental facilities with optical access, appropriate light detection instrumentation, and potentially external light sources and delivery optics. Three types of optical facilities that recreate engine-relevant high-pressure, high-temperature conditions are reviewed here: engines, rapid compression machines, and pressurized high-temperature spray chambers. Also, several of the more commonly applied optical diagnostic techniques that can detect combustion-generated light emission, attenuation and scattering of light from external sources, and artificially generated emission, including laser-induced processes, are also briefly reviewed.

1. OPTICAL ENGINES AND OTHER FACILITIES

1.1 Optical Engines

An optical engine is designed with transparent windows to allow processes occurring inside the cylinder of the running engine to be viewed. A normal production metal engine may be modified for optical access, or a stand-alone optical engine may be specifically designed for the task. With optical access, not only can the cylinder contents be passively observed, but laser-based measurement techniques may also be applied to extract specific information about the physical and chemical in-cylinder processes occurring rapidly in the harsh, high-pressure, high-temperature environment inside the engine.

Optical access to combustion chambers can be created in different ways and to different extents. Small-scale (a few millimeter) windows can accommodate laser-beam input and endoscopic viewing through the cylinder head or cylinder wall, while large-scale (tens of mm or more) windows can provide access to the whole cylinder liner (using a toroid window) or the piston-top (using a disk window) for full-field imaging. In keeping with the generally accepted meaning of “optical engine” within the engine research community, this section describes engines with large-scale optical access that requires significant engine modifications.

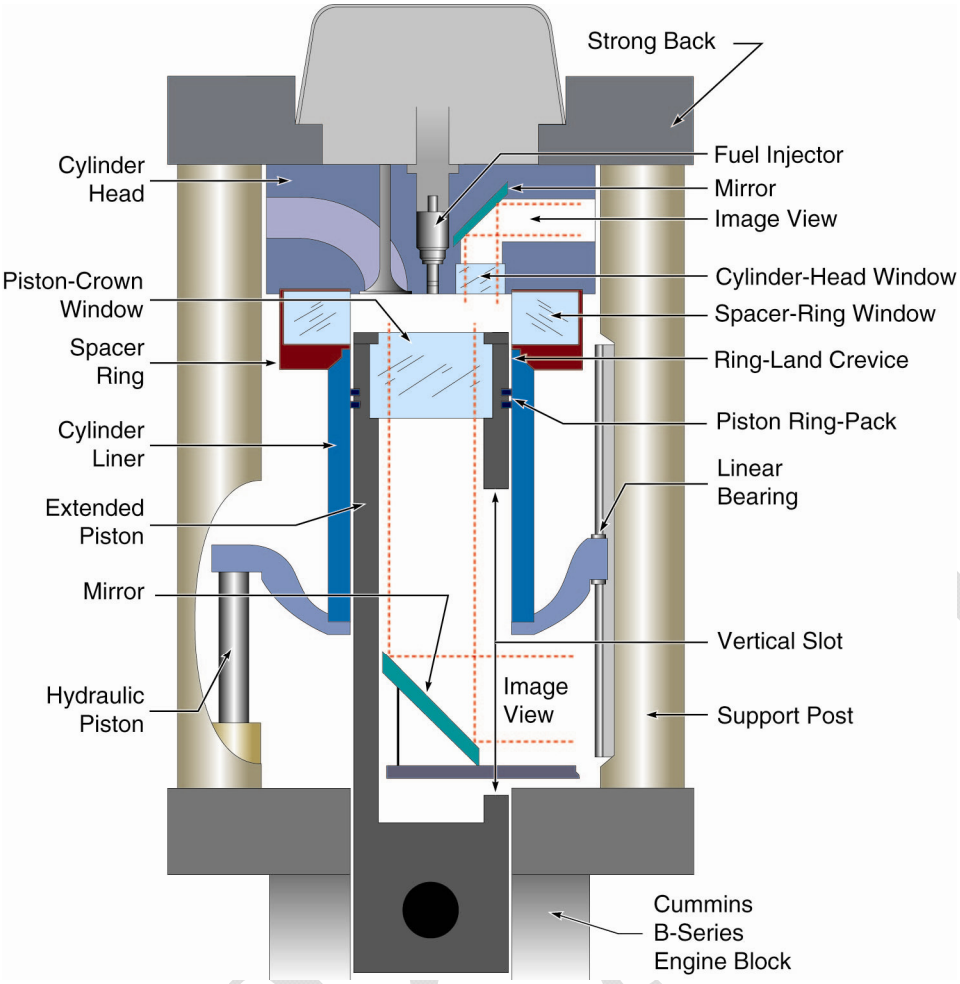

Figure 1. Schematic example of an optically accessible engine with piston extension (and cylinder-head window illustrated, adapted from [1]). All key components of the upper engine are shown. The base engine block (here a Cummins B-series) is below, with its optical piston extending upwards into the optically accessible part of the engine.

Optical engines are typically single-cylinder versions of multi-cylinder production engines. A typical example of a modern design with optical access through the cylinder liner. piston crown, and cylinder head is shown schematically in Figure 1. The key features are as follows:

- Optical access through a spacer ring with flush-mounting, curved spacer-ring windows. Typical window materials are fused silica (excellent UV light transmission) or sapphire (ultra-hard and strong).
- Correspondingly lowered piston ring-pack keeping the rings from sliding over the windows (but also creating a large ring-land crevice volume and lower compression ratio).
- Piston rings from self-lubricating polymer mixtures to allow operating the upper engine nearly oil-free. Oil would greatly contribute to window fouling.

- Optical access through a window in the piston crown, which forms the top part of an extended piston with a tall vertical slot for viewing access ("Bowditch" piston [2]).
- A stationary mirror at 45°, inserted from the side into the piston slot, allowing upwards viewing through the piston window at all times in the cycle.
- Additional small-scale windows and mirror in the engine head, for example inserted in place of one of the exhaust valves. Figure 10 originates from such an arrangement.
- A means of quickly separating the engine head from the cylinder liner to allow for cleaning the inside surfaces of windows. Here, the cylinder liner can be lowered and raised hydraulically. Other solutions exist.
- A stiff connection of the base engine's crank case to the cylinder head, which is elevated due to the extended piston. In Figure 1, four massive support posts are bolted to a "strong back" that holds the cylinder head down against the cylinder pressure and upward force from the hydraulic pistons that hold the liner tight against the cylinder head.
- A base engine providing the piston kinematics and forces. For the engine in Figure 1, the first cylinder of a suitably modified six-cylinder block is used. More typical bases are robust single-cylinder research engines.

Many variations of the concept outlined above are possible. Perhaps the most important ones pertain to the optical ports. Compared to Figure 1, other designs have

- A short transparent ring instead of the metal spacer with small windows. This large-scale window option gives 360° optical access to the top 10-20% of the combustion chamber, but limits the safe peak pressure to about 50-100 bar.
- A full-height transparent liner with the piston rings sliding over the liner. This configuration provides 360° optical access to the entire piston stroke, but it is much more fragile than other designs and is almost exclusively used in motored operation only.
- No piston-crown window. Particularly for laser-based imaging this severely limits the possible configurations, but also obviates the need for a piston extension.

Due to the optical access modifications, the many aspects of optical engine performance differ from those of a similar production engine. Replacing liquid-cooled metal components with largely uncooled windows having different material properties alters the heat transfer between walls and the gas phase. Additionally, oil-free polymer piston rings can have much more blow-by than their production metal counter-parts. Gapless rings can help to reduce blow-by, but their friction is very temperature-dependent because they expand significantly when heated. Polymer rings, limited cooling, and lower thermal gradient tolerance of optical materials limit the thermal load the engine can tolerate, so optical engines are often "skip-fired." In this mode of operation, one or several fired cycles for data acquisition are followed by (~10) motored cycles to allow the engine and optical components to cool down somewhat. With skip-firing, engine systems that use the exhaust gas stream, like turbocharging or exhaust-gas recirculation (EGR), cannot

function as in a normal engine. To simulate turbocharging or EGR, optical engines typically are supplied with an externally pressurized and heated mixture of air with nitrogen, carbon dioxide, and/or water vapor and other gases properly metered to mimic EGR.

Further limitations in the operating range come from the mechanical properties of the optical materials (fused silica or sapphire), which are reasonably strong, but very brittle, with a low coefficients of thermal expansion that are mismatched with most metals. When an extended piston is used, the additional weight of the piston not only requires redesign of the engine's mass balancing, but also a reduction in maximum speed. Typical top speed of a light-duty optical engine may be 2000 – 2500 rpm, compared to 5000-8000 for similar metal engine designs. Together with blow-by, the reduced axial stiffness of the slotted, extended piston also means the real compression ratio can be significantly different from the geometric compression ratio {Kashdan, 2009 548 /id}. Particularly the calculation of apparent heat-release rate is affected by this [4,5]. Adjusting intake temperature and pressure allows matching thermodynamic conditions of the intended all-metal counterpart over a limited range of crank angles, which may be sufficient to study for example injection and ignition in Diesel combustion under realistic conditions [6].

Finally, because of these thermodynamic differences and often much greater crevice volumes, exhaust gas composition will also differ from that of a nominally identical all-metal engine. With careful operation, however, trends over a parameter variation can be reproduced well with an optical engine [6].

1.2 Rapid Compression Machines

A rapid compression machine (RCM) is similar to an engine, in that it features a closed cylinder with a sliding piston that compresses gases within the cylinder. Unlike an engine, however, the RCM is designed so that the piston remains stopped at the end of compression, so that the compressed gases do not expand. The compressed gases thus remain at high temperature and pressure for an extended period of time (10-100 ms), during which in-cylinder processes may be studied.

Optical RCMs generally share the same five operational elements: a "driver section" that applies force to accelerate a sliding piston, a closed piston-cylinder "driven section" in which gases are compressed, a mechanism to decelerate and hold the piston, a compression (combustion) chamber at the end of the piston's stroke, and transducers/windows for optical and other diagnostics. A schematic representation of the operation of one RCM, based on a design from the University of Michigan [7], is shown in Figure 2. Many other designs for RCMs exist, a number of which are listed in Table 1.

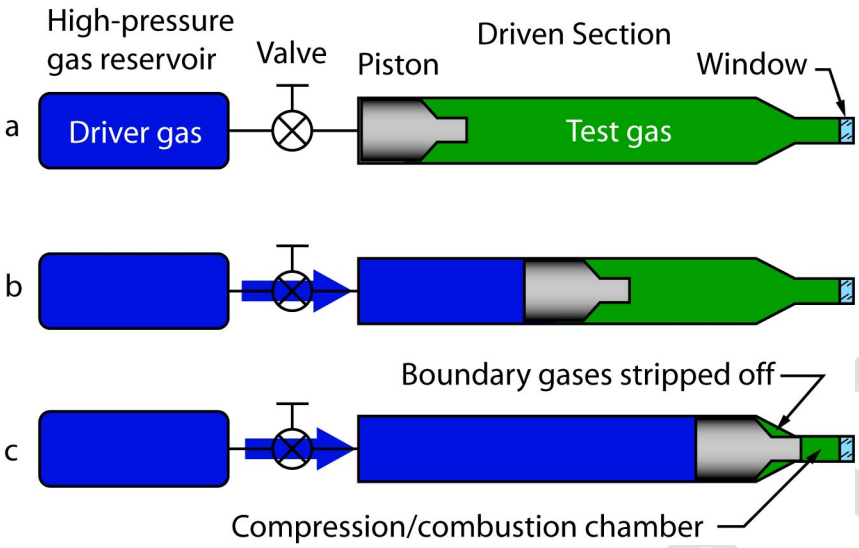

Figure 2. Example of RCM operation for design similar to that of University of Michigan [7]: (a) the driven section is filled with the test gas (green) to be compressed. (b) a control valve is opened to release high-pressure gas (blue) that accelerates piston, which compresses the test gas mixture. (c) at the end of its travel, the piston decelerates and locks in place as it wedges into the end of the driven section. Cooler and more turbulent boundary gases are stripped off into the shoulder region outside the compression/combustion chamber.

Table 1: Brief summary of a number of RCMs

Institution	Acceleration/ Deceleration	Bore [mm]	Comp Time [ms]	Comp. ratio	Reference
U. of Michigan	pneum./ wedge	50.8	70	37	CNF 137:351-65, 2004
Mass. Inst. Tech.	pneum./ hydr.	50.8	10-30	19	CNF 132:219-39, 2003
Hosei Univ.	pneumatic	80	-	-	SAE 2001-28-0010
U. P. et M. Curie	hydraulic	40	29	15	SAE 2007-01-1869
University of Leeds	pneum./ hydr.	45	22	14.6	CNF 39:255-268, 1980
U. Sci. Tech. Lille	pneum./ cam	50	60	10	PCI 23:1753-58, 1990
Nihon U.	collision/crush	56	5	18.7	SAE 2008-01-2403
Keio U.	pneum./ hydr.	145	185	14.6	SAE 2009-32-0085
U. Tokushima	pneumatic	60	-	-	SAE 2003-01-1792
Norw. U. Sci. T.	hydraulic	80.5	-	11.2	SAE 2005-24-009
Seoul Nat. U.	hydraulic	60	20	20	SAE 2007-01-0218
Kyushu U.	pneum./ cam	50	53	22.4	SAE 2002-01-2867
Tokyo Inst. Tech.	-	200	-	14.7	SAE 811004
Tech. U. Lodz	pneumatic	60	20	16	SAE 2001-01-1338
Nagoya Inst. Tech.	-	65	20	~5	COMODIA:189,1994
U. Tokyo	pneum./ lock	50	10	12.2	CNF 54:33-47, 1983
Honda	pneum./ cam	80	50	16.1	SAE 2007-01-2038
Gunma U.	pneum./ lock	80	55	10	SAE 2005-26-358
U. Karlsruhe	pneumatic	88sq	-	6	SAE 2005-01-0238
Wayne State U.	pneum./ hydr.	38	-	~19	SAE 2001-01-2005
Argonne N. Lab.	pneum./ hydr.	63.5	17	12	SAE 2005-01-2189

The RCM driving system is typically pneumatic or hydraulic, and it can act on the piston directly, as in Figure 2, or it can drive a second piston-cylinder arrangement that is mechanically connected to the compression piston. Other less-common driving systems include mechanical cams/ramps or even gravity-driven free-fall/impact. After compression, the piston must be decelerated at the end of its stroke and held in place to maintain compression. Deceleration may be accomplished by crushing/wedging elements as in Figure 2, by controls on the drive side, or by hydraulic or pneumatic braking. Piston rebound after deceleration also must be avoided to maintain compression, either by wedging elements that hold the piston tight (Figure 2), feedback control of the driver system, or mechanical locks.

RCMs are often utilized to study chemical kinetics, for which it is desirable to create a uniform gas temperature and composition as quickly as possible. Pre-compression non-uniformities, heat losses creating cooler gases near the cylinder wall, and flows generated by compression all can contribute to non-uniformities in the compressed gases. Some RCM designs, such as the one illustrated in Figure 2, use a tapered/stepped piston to strip off the cooler and more turbulent boundary gases and prevent them from entering the compression chamber, thereby improving charge uniformity.

Most RCM compression times vary from 20 to 200 ms, while engine compression times range from to 5 to 50 ms for crankshaft speeds from 600 to 6000 rpm. The fastest RCM listed in Table 1, from Nihon University in Japan [8], uses a piston-collision design to generate a rapid 5 ms compression time. RCMs typically measure the piston position and velocity during the compression stroke for diagnostics and/or feedback control of the driver system. Optical access to the compression/combustion chamber is typically achieved with either a large-scale disk-window at the top of the compression chamber, or by full large-scale optical ring or small-scale windows around the side of the compression chamber.

Further reading:

Guibert, P., Keromnes, A. and Legros, G., “Development of a turbulence controlled rapid compression machine for HCCI combustion,” SAE paper 2007-01-1869, 2007.

1.3 Static High-Temperature, High-Pressure Spray Chambers

While experimentation in optical engines and rapid compression machines simulates the time-history of compression of practical engines, uncertainties in the charge gas temperature and EGR distribution at the time of fuel injection can be significant. Consequently, the details of combustion that unfold can also have significant uncertainty. Furthermore, the maximum pressures and temperatures achievable in reciprocating optical facilities is limited, as discussed in section 1.1. As an alternative, devices that generate sustained charge-gas conditions typical of full compression have been developed, intending to isolate certain variables and to provide a more fundamental understanding of spray combustion than can be achieved in engine experiments, and at more extreme operating conditions. Fundamental understanding over a wide range of

conditions is especially needed for development of improved CFD models where specification of exact boundary conditions is critical.

A schematic for a typical high-temperature, high-pressure spray chamber is shown in Figure 3. The chamber shown is cube-shaped with ports available on the six faces of the cube. In Figure 3, the chamber is configured with four optical windows to allow full view of the spray, either by line-of-sight, head-on, or side access. A custom fuel injector with a single axial hole is mounted in one of the other ports, producing a spray that penetrates into the middle of the chamber. Intake and exhaust of gases occurs via small valves located at the chamber corners. The valves are closed during injection such that flow within the vessel is mainly generated by the spray itself. While highly simplified, this type of static chamber offers advantages in terms of optical access, maximum pressure and temperature capability, and isolation of variables compared to a running engine configuration.

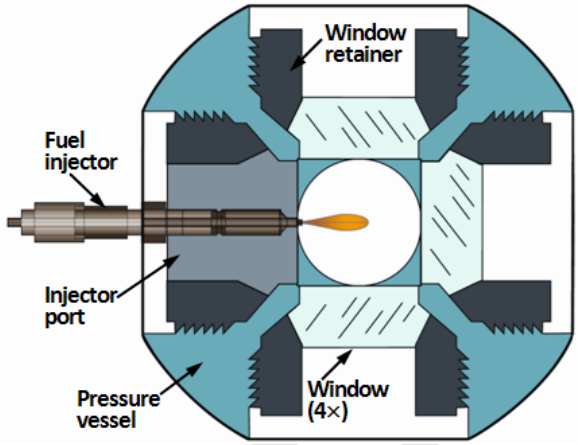

Figure 3. Schematic of high-temperature, high-pressure constant-volume preburn chamber [9].

The operational challenge for these types of chambers is to simultaneously generate high-pressure and high-temperature conditions representative of engines at full compression. Several different approaches have been developed, each with different design tradeoffs and capabilities. A summary of current device capabilities in terms of pressure and temperature is given in Table 2.

Table 2: Summary of reported constant-volume heated (CVH), constant-pressure flow (CPF), and constant-volume preburn (CVP) chambers.

Institution	Type	Max. T [K]	Max. P [bar]*	Reference
Colorado School Mines	CVH	873	50	Rev.Sci.Inst.76(3):035108 (2005)
Doshisha U.	CVH	700	30	SAE 2004-01-0529
Hiroshima U.	CVH	873	41	SAE 1999-01-3600
Paul Scherrer Inst.	CVH	850	80	Appl.Phys.B 80:1039 (2005)
RWTH Aachen U.	CPF	800	50	SAE 2007-01-0020
Caterpillar	CPF	1000	150	ILASS 2011-177
Chalmers U.	CPF	900	100	SAE 2004-01-1917
CMT U. Pol. Valencia	CPF	1000	140	ILASS 2011-163

U. Erlangen	CPF	1000	100	SAE 2011-01-1928
General Motors	CPF	900	100	ILASS 2011-170
Brigham Young U.	CVP	1400	100	SAE 2005-01-0381
Doshisha U.	CVP	1400	100	SAE 2003-01-0073
Eindhoven U.	CVP	1400	350	SAE 2009-01-0649
Ghent U.	CVP	1400	350	SAE 2012-01-0461
IFP Energies Nouvelles	CVP	1400	150	SAE 981069
U. Illinois U.-C.	CVP	1400	180	SAE 2004-01-1411
Kyoto U.	CVP	1400	150	SAE 2005-01-0364
Mich. Tech. U.	CVP	1400	350	ASME ICEF2011-60034 (2011)
N.C. State	CVP	1400	70	SAE 2011-01-1380
Sandia	CVP	1400	350	SAE 980809
Seoul Nat. U.	CVP	1400	60	SAE 2011-01-0684
Tokyo Tech./Meiji U.	CVP	1400	80	IJER 11:79 (2011)
U. Wisconsin	CVP	1400	100	SAE 2001-01-3495

SAE=Society of Automotive Engineers, ILASS=Institute for Liquid Atomization and Sprays, ASME ICEF=American Society of Mechanical Engineers Internal Combustion Engine Fall Conference, IJER = International Journal of Engine Research

*Maximum pressure: stated design or maximum demonstrated

The first type of device listed is constant-volume heating (CVH), wherein the gases are directly heated by the walls of the chamber or by heating elements placed inside a closed chamber. An alternative is to highly preheat gases and quickly ingest them into the chamber before valve closure. Either way, the vessel walls must be heated significantly. Because of the high optical and metal material temperature, and associated lower mechanical strength, the maximum pressure and temperature rating for these devices tends to be relatively low. Table 2 indicates that CVH design ratings fall below 80 bar and 900 K, which does not encompass the full range applicable to engines. Another disadvantage is that significant time (~10 min.) is typically required to prepare a single charge, which limits the rate of experimentation.

The second approach listed is constant-pressure flow (CPF). For these devices, the system is open and controlled to a specific pressure. A flow of hot, pressurized gases is continuously delivered to the injector region. Fuel is injected into these gases periodically and then naturally scavenged away from the injector by the flow of air. Like CVH chambers, a significant challenge is attaining high-temperature and pressure conditions because of material limitations. A solution is to separate and insulate components that direct the flow of high-temperature gases from that of a cooled, outer pressure vessel, thereby creating a double-hull structure of hot and cold windows and housing. Table 2 shows that temperatures as high as 1000 K, and pressures as high as 150 bar are possible with this type of CPF design. A substantial benefit of a CPF chamber is that injections may be repeated quickly (~one per second), permitting fast experimentation.

The third device is a constant-volume preburn (CVP) chamber, which is the type depicted in Figure 3. Table 2 shows that CVP chambers have been designed to reach temperatures of 1400 K and pressures as high as 350 bar, which is significantly higher than either CVH or CPF chambers. CVP chambers use spark-ignition and combustion of a premixed, fuel-

lean mixture to raise the temperature within the vessel [10]. The gases and walls may be preheated, as in CVH or CPF designs, but it is the "preburn" combustion that primarily raises the temperature and pressure. Chamber wall and gas heating to only 450-500 K is typical, while lean flame temperatures approach 2000 K. Because of this temperature differential, the preburn combustion products cool over time and the vessel pressure and temperature slowly decrease. Fuel injection may occur at anytime during this cool down when the desired pressure and temperature is reached, thereby producing an extensive range of possible gas states at the time of injection. However, in practice a time delay after completion of the premixed burn is needed to finish reaction and produce a more homogenous gas core to mix with the spray, hence the upper estimate of 1400 K for peak temperature listed in Table 2 is lower than the lean flame temperature of about 2000 K.

For CVP chambers the composition of the initial reactant mixture is chosen so that, following its complete combustion, the product gas composition simulates air (21% O_2) or even EGR-diluted engine intake conditions (e.g., 10-19% O_2). As such, the spray will autoignite as it does in diesel combustion. Alternatively, a preburn mixture that yields 0% O_2 can be produced to simulate high-temperature and pressure conditions, but since the mixture is inert, no combustion occurs. In this way, the spray mixing and vaporization processes may be separated from that with ignition and combustion. While CVP chambers can traverse a wide range of temperature, pressure, and ambient composition compared to other devices, a disadvantage is that the preparation steps to produce the preburn take several minutes, thereby limiting the rate of experimentation, particularly compared to continuous-flow CPF chambers.

Further reading:

Baert, R., Frijters, P., Somers, B., and Luijten, C., "Design and operation of a high pressure, high temperature cell for HD diesel spray diagnostics: guidelines and results," SAE Paper 2009-01-0649, 2009.

Engine Combustion Network. http://www.sandia.gov/ECN

2 OPTICAL DIAGNOSTIC TECHNIQUES

A variety of in-cylinder phenomena may be probed by optical diagnostics, including: flow structures and turbulence associated with gas exchange, compression/expansion, and transient fuel jets; liquid-fuel atomization and vaporization; mixing of vapor fuel with ambient gases; ignition and combustion; and pollutant formation and destruction. The light measured by the optical diagnostics may arise naturally from combustion processes, or it may be artificially introduced and/or induced using external light sources, including lasers, flashlamps, arcs, and light-emitting diodes. Many optical diagnostics are available, and it is beyond the scope of this article to present all of them. The following is a brief overview of several of the more commonly used diagnostics.

2.1 Naturally Occurring Luminescence

Combustion processes emit light from chemical reactions (chemiluminescence) and combustion-heated particles may also emit light (incandescence). Both the intensity and the spectrum (color) of the naturally occurring luminescence can provide information about the local temperature and concentration of the emitters.

2.1.1 *Chemiluminescence*

Chemical reactions during combustion can either emit light directly, during the reaction, or indirectly, buy producing electronically excited species that later emit light when they spontaneously return to an electronic ground state. For direct chemiluminescence, excess reaction energy is emitted as light (photons). One important direct chemiluminescence reaction is the CO continuum:

$$CO + O \rightarrow CO_2 + hv \quad (1)$$

In equation (1), *hv* represents the emission of a photon from the reaction. The wavelength (color) of the emitted photon depends on the excess energy in the reaction collision, which is not quantized. Hence, the photon wavelength can vary continuously. In the case of the CO continuum, the emission is in the blue to ultraviolet, over the approximate range from 350 to 450 nm.

For other chemiluminescence reactions, excess chemical energy is not released immediately, but rather it is temporarily stored in the electron cloud of one of the product species. A few important reactions producing electronically excited species are:

$$CH + O_2 \rightarrow CO + OH^* \quad (2)$$

$$C_2 + OH \rightarrow CO + CH^* \quad (3)$$

$$CH_2 + C \rightarrow H_2 + C_2^* \quad (4)$$

$$CH_3O + OH \rightarrow HO_2 + CH_2O^* \quad (5)$$

In equations (2-5), the "electronically excited" species are denoted by an asterisk superscript. In the excited species, one electron occupies a quantum manifold (shell) that is one or more electronic levels above the lowest, or ground manifold. The electron does not remain in the excited manifold indefinitely, but rather spontaneously "relaxes" to a lower (usually ground) manifold, and in doing so, emits a photon. Both the excited and ground manifolds can have a multitude of slightly different, yet discrete (quantized), energy states, depending on the vibrational and rotational quantum numbers of the occupied states. The spontaneous transition of each excited molecule must occur between discrete quantum states. As a result, the wavelength (color) of the emitted photon must correspond exactly to the energy difference between the two states. Among the population of all emitting molecules in a probed region, many different transitions will occur between many different vibrational and rotational states, so that the collection of emitted photons will have many different, yet discrete, colors. The chemiluminescence emission thus bears the spectral "fingerprint" of the excited species.

The intensity of chemiluminescence emission depends on the reaction rate and/or the concentration and temperature of the emitters. High-temperature combustion reactions that produce CH*, OH* and C_2* are often detectable with photodiodes or unintensified cameras at bandwidths or frame-rates on the order of 10 kHz. For weaker low-temperature (cool-flame) combustion reactions, emission from CH_2O*, or for conditions with weaker high-temperature reaction emissions (e.g., with dilution by exhaust gases, or late in combustion), photomultiplier tubes or intensified cameras may be required.

A few notable examples of chemiluminescence measurements are: using chemiluminescence of OH* as a marker for high-temperature reactions in diesel sprays to measure the lift-off length [9]; using relative CH*, C_2*, and OH* chemiluminescence

intensities to infer the local equivalence ratio [11]; and tracking ignition and combustion in compression ignition engines [12,13].

Limitations of chemiluminescence include the line-of-sight nature of the signal and interference by other emitters. Emitters all along the line of sight contribute to the emission that reaches the detector, so that the signal represents an accumulation along the line of sight. Hence, two-dimensional images are effectively projections of a three-dimensional source. Spectral measurements also represent an integration along the line of sight. Spectral filters or dispersion techniques (e.g., spectrographs) can help to isolate specific emitting species, but the spectral emission of multiple species often overlap, which limits the specificity of the chemiluminescence signal. Furthermore, other emission sources, especially including soot incandescence, can be orders of magnitude stronger and overlap spectrally with the chemiluminescence emission.

Further reading:

Gaydon, A.G., *The spectroscopy of flames*, 2nd ed., Chapman and Hall, 1974.

Nori, V. and Seitzman, J., "Evaluation of chemiluminescence as a combustion diagnostic under varying operating conditions," AIAA paper 2008-953, 2008.

2.1.2 Soot incandescence

Under fuel-rich conditions, combustion reactions can synthesize carbonaceous soot particles, some of which survive combustion and are ultimately exhausted from the engine, along with adsorbed hydrocarbons and sulfates, as particulate matter (smoke). (See Article 8 for more information about particulate matter.) The soot is of practical interest because it is a primary component of particulate matter, and emissions of particulate matter from engines are regulated in most markets. Hence, knowledge of the in-cylinder processes that control the formation and destruction of soot is important for designing combustion systems that comply with air quality standards.

While inside the engine, the combustion-generated soot particles are heated to high temperatures such that they glow by incandescence. In an aerosol (cloud) of soot particles, some of the light emitted by each particle is scattered and absorbed by other particles, and the amount of absorption and scattering within the cloud depends on the amount of soot and on the light wavelength. The spectral intensity of light that is ultimately emitted by a soot aerosol cloud can be approximated as a fraction ε (emissivity) of that of a blackbody, according to the Planck equation:

$$I = \varepsilon \frac{375\left[W \cdot nm^2\right]}{\lambda^5\left(exp\left(\frac{14.4 \cdot 10^6\left[nm \cdot K\right]}{\lambda T}\right) - 1\right)} \tag{6}$$

In the above equation, I is total the spectral intensity in W per nm^3 (radiative power per source area per wavelength) emitted into a hemisphere, λ is the light wavelength in nm, T is the soot temperature in K, and ε is the emissivity (which would have a value of one at all wavelengths for a blackbody).

Assuming scattering is negligible, the emissivity of the aerosol soot cloud ε can be expressed as

$$\varepsilon = 1 - \exp(-k_a L) \quad (7)$$

where k_a is the soot absorption coefficient, and L is the path length of the light traveling through the cloud. The product k_aL is often termed the "KL" factor. The absorption coefficient depends on both the soot concentration and on the soot optical properties, which vary with the light wavelength. Various approaches, either fundamental or empirical, can provide a functional relationship between k_a and soot concentration. The optical properties of soot and the importance of scattering are highly uncertain, however, which translates to high uncertainty in the relationship between k_a and soot concentration. Nevertheless, using the two above equations together, the broadband spectrum and intensity of the soot aerosol emission thus becomes characteristic of the soot temperature and concentration. Hence, simultaneous measurements at multiple light wavelengths can provide sufficient information to determine both the soot temperature and its concentration. Measurements at a minimum of two wavelengths are required, which yields two equations for the two unknowns (temperature and concentration).

Figure 4 shows an example of soot KL and temperature maps for n-heptane diesel spray combustion [14]. The KL and temperature data were calculated from two-color soot incandescence images acquired with a single color camera with relatively broad blue (400-550 nm) and red (570-700 nm) channel sensitivities. The 2-color data were compared with laser-extinction measurements of soot (see section 2.3.1), which showed that the 2-color KL values were consistently lower than the extinction measurements, though the trends were consistent.

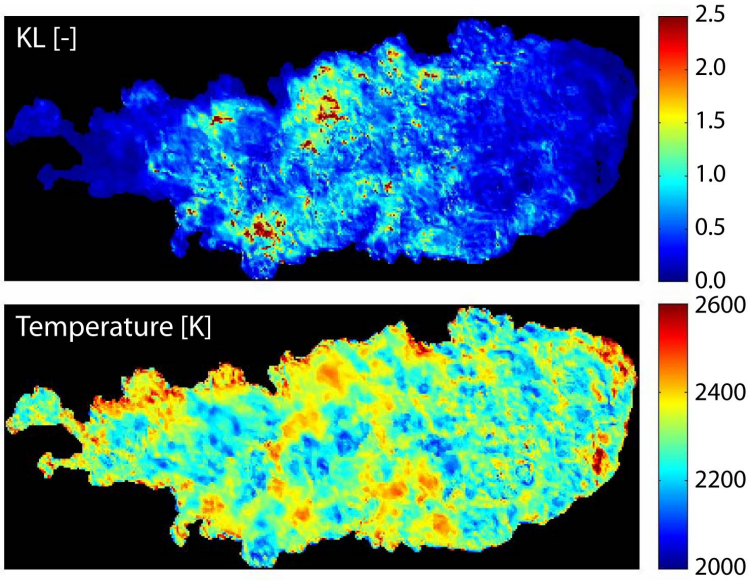

Figure 4. Soot KL and temperature in an n-heptane diesel jet measured by the two-color method [14].

In addition to the study in Figure 4, a few other notable examples of soot incandescence measurements are: total soot incandescence imaging of diesel soot [15]; total soot incandescence, two-color, and laser-induced incandescence imaging in diesel spray flames [16];and two-color uncertainty assessment with computer modeling and measurements under conventional and low-temperature diesel combustion conditions [17].

While broadband measurements (imaging) of the soot emission can provide some information about in-cylinder soot formation and destruction, the data are confounded because variations in soot intensity may be due to variations in either soot concentration or temperature, or both. Two-color techniques, in theory, can separate the temperature and concentration effects on the emission intensity, so that soot formation and destruction can be quantified. In practice, however, the measurement uncertainty can be considerable. In addition to uncertainty in the soot optical properties and absorption and scattering processes, variations in the soot temperature along the line of sight, additional extinction from window deposits, and the contribution of reflections off in-cylinder surfaces and other luminous interferences can further increase the uncertainty. One other laser-based option for measuring temperature in engines is coherent anti-Stokes Raman spectroscopy (CARS). The technique is based on interaction of several laser beams in the probe volume and yields highly resolved anti-Stokes Raman spectra of (usually) nitrogen, which are fit to calculated data to obtain temperature. Its main advantages are high accuracy, broad applicability, and resistance against interfering signals. To its disadvantage, it is mature only as a point measurement and data evaluation requires a relatively high degree of spectroscopic expertise. A recent application example is [18].

Further reading:

Zhao, H. and Ladommatos, N. “Optical diagnostics for soot temperature measurement in diesel engines,” Progress in Energy and Combustion Science 24, 221-255, 1998.

di Stasio, S. and Massoli, P. “Influence of the soot property uncertainties in temperature and volume-fraction measurements by two-color pyrometry,” Measurement Science and Technology 5, 1453-1465, 1994.

2.2 Beam refraction: Shadowgraphy & Schlieren

Variations in local density and composition in combustion systems and evaporating sprays create gradients in the refractive index, so that light passing through the region is bent. Optical techniques sensitive to refractive index gradients can probe such regions. Schlieren and shadowgraph imaging systems exhibit different sensitivities to the variations in refractive index, and are conveniently applied wherever there is line-of-sight optical access. The lighting and imaging arrangement also lends itself easily to high-speed imaging, wherein the entire cycle or injection and combustion event can be resolved with hundreds or thousands of images.

A Z-type schlieren or focused shadowgraph setup may utilize inexpensive lighting, such as lamp or LED point sources, coupled to camera imaging systems [19,20]. The diverging point-source light is collected and collimated by a concave mirror, passed through the combustion chamber, re-focused using a second concave mirror, and then directed into a camera equipped with lenses appropriate for the desired image magnification.

Schlieren stops are placed at the collection focal point to adjust system sensitivity to refractive index gradients. A knife edge is the classic schlieren stop. When rays are steered by refractive index gradients within the combustion chamber, they may be steered into or away from the knife edge, thereby identifying these regions in the collected image. The degree of knife-edge cutoff affects the sensitivity. With 0% cutoff (no knife edge), the sensitivity is weakened and the system is technically no longer a schlieren

setup, but rather a “focused shadowgraph” [19]. With high cutoff, the sensitivity to refractive index gradients increases. A round aperture can be used as a schlieren stop producing a “bright field”, since it tends to leave the background bright, and darken regions where there is a schlieren effect. Alternatively, a full light cutoff at the focal spot with a pin shape produces a “dark field” because schlieren-effected regions appear bright above a dark background.

For vaporizing fuel sprays, schlieren imaging shows the boundary between vaporized fuel and background ambient gases because (1) refractive index differences exist between the fuel and ambient gases and (2) density gradients are created in the ambient gases as the vaporized fuel spray cools the ambient. An example is shown in Figure 5. The technique also works well to identify the boundary of non-vaporizing sprays because of light extinction by droplets [21] (see Article 2.3.2). Light extinction by droplets is clearly shown in the upstream region of the spray in Figure 5. Strong density (and refractive index) gradients are also easily detected at combustion interfaces as high-temperature combustion forms distinct low-density regions. In addition, first-stage ignition in a fuel jet, where the parent fuel breaks down and the temperature rises only modestly, produce a vanishing schlieren effect as these ignition steps change the refractive index of the jet to match the ambient more closely [20].

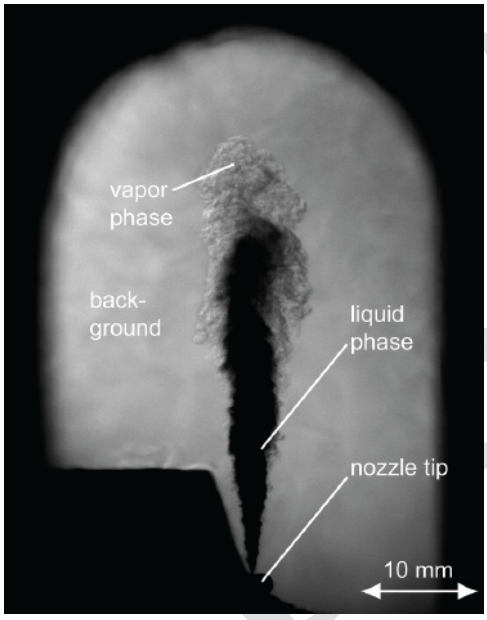

Figure 5. Schlieren imaging of a diesel spray penetrating into ambient gases at 800 K and 50 bar [22].

Further reading:

Settles, G.S., *Schlieren and Shadowgraph Techniques*, Springer-Verlag, 2001.

2.3 Beam extinction

Light passing through an engine combustion chamber may be absorbed and/or scattered by the in-cylinder contents. The sum of absorption and scattering, termed “extinction,” can be indicative of the properties and quantity of matter along the beam path. The transmitted intensity of a light beam directed through the combustion chamber can be

measured to quantify the amount and/or temperature of in-cylinder soot particles, liquid fuel sprays, and in-cylinder gases.

2.3.1 Soot

The transmitted intensity I of a light beam passing through a uniform soot cloud (aerosol) can be described by the Beer-Lambert law:

$$I = I_0 \, exp(-k_e L) \tag{8}$$

In the above equation, I_0 is the incident intensity of the light entering the soot cloud, L is the path length of the light passing through the cloud, and k_e is the extinction coefficient, which can include both scattering and absorption.

With measurements of the incident and transmitted intensities, the value of k_eL, often called the "KL factor," can be determined using equation (8). The KL factor is a relative measure of the amount of soot along the path of the beam. An absolute measure of the soot may be estimated using correlations for k_e that are either empirically based or from scattering theory using the optical properties of the soot particles. For small soot particles, extinction is typically dominated by absorption, such that the extinction coefficient in equation (8) can be approximated as the absorption coefficient k_a used in equation (6) of the two-color incandescence method.

The light source for extinction measurements is usually a laser source, though other light sources could be used as well. Figure 6 shows soot KL measurements in a diesel spray flame using n-heptane fuel at several different ambient oxygen concentrations [23]. The data are plotted versus the "flame coordinate," which is the reciprocal of the nominal equivalence ratio along the jet axis. The data show how soot is formed and consumed along the jet axis, and how dilution by EGR reduces soot formation.

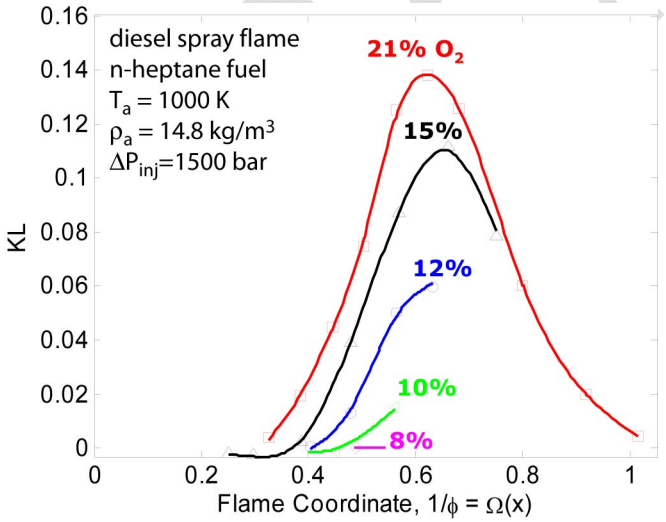

Figure 6. Laser-extinction measurements of soot KL in a diesel spray flame using n-heptane fuel at different ambient oxygen concentrations, plotted as a function of flame coordinate [23].

In addition to the study highlighted in Figure 6, a few notable examples of soot extinction measurement are: combined soot extinction and laser-induced incandescence in a gasoline direct injection engine {de Francqueville, 2010 537 /id}, fundamental soot extinction measurements in several laminar diffusion flames [25], and a modified

forward-illumination extinction technique that can be particularly useful in engines with limited optical access {Xu, 2005 538 /id}.

Properly applied, the soot extinction technique can provide quantitative measurements with relatively low uncertainty, and hence it has been used frequently as a calibration for other soot measurement techniques. Nevertheless, many of the same uncertainties in the soot optical properties and window transmission involved in the two-color soot incandescence measurements described in section 2.1.2 also must be considered in the functional relationship between the KL factor and the total soot mass or volume fraction along the beam path. Furthermore, the technique usually needs to be designed to minimize interference from combustion luminosity, and the sensing optics must accommodate any bending of the extinction beam that may occur as it passes through regions of varying density within the combustion chamber.

Further reading:

Musculus, M.P.B. and Pickett, L.M., "Diagnostic considerations for optical laser-extinction measurements of soot in high-pressure combustion environments," Combustion and Flame 141(4), 371-391, 2005.

Zhao, H. and Ladommatos, N. Engine Combustion Instrumentation and Diagnostics, chapter 11, Society of Automotive Engineers, 2001.

2.3.2 Sprays

Like soot, fuel spray droplets cause light extinction of transmitted laser beams or other light sources. The attenuation of light is a convenient diagnostic to characterize the spray position and concentration of droplets, or to determine the position where all liquid droplets are vaporized as they mix with hot, in-cylinder gases. Liquid droplet extinction is labeled in the vaporizing spray of Figure 5. Another example of light extinction in a low-temperature hollow-cone gasoline spray is given in Figure 7. Rather than a collimated light source, as with a laser beam or schlieren imaging (2.2.1), in this case the spray is illuminated from the back with a diffuse light source [27,28]. Dark regions indicating light extinction by droplets are readily apparent.

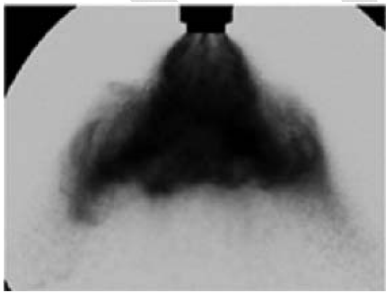

Figure 7. Diffuser back-illumination image of an air-assist gasoline spray [27].

Quantifying the total liquid fuel volume along the light path is difficult because of complex extinction relationships for fuel droplets. The measured intensity and the Beer-Lambert law (Eq. 8) can be applied to assess the extinction coefficient k_e for a cloud of droplets, with $k_e = \sigma_{ext} N$ where σ_{ext} is the extinction cross-section of a droplet and N is

the number density of droplets. But fuel droplets have much different σ_{ext} characteristics compared to soot particles. Fuel droplet extinction is dominated by light scattering, rather than absorption. In addition, fuel droplet size is much larger (tens of μm) than that of soot particles (tens of nm). As shown in section 2.4.1, Mie-scatter theory predicts significant changes in σ_{ext} depending upon the size of the particle/droplet, thereby making quantification difficult, especially since droplet size is non-uniform in most applications. Another challenge is that many engine sprays are dense, with either high σ_{ext} or N, causing nearly complete extinction, as well as multiple-photon scattering with illumination originating from many directions other than the original source. Techniques to suppress multiple scattering are therefore being developed and applied, both with advanced laser systems [29,30] and x-ray sources [31]. While difficult to quantify the fuel volume within the spray, light extinction is particularly useful for rapid characterization of the spray envelope as depicted in Figure 7.

Further reading:

Gasoline Fuel Injector Spray Measurement and Characterization, SAE standard J2715, SAE, 2007.

2.4 Elastic Scattering

Direct elastic scatter from laser or other light sources is applied to characterize in-cylinder fuel-air mixing, liquid evaporation, and combustion. Unlike the diagnostics covered thus far in previous sections, light collection at angles to a precisely directed light source, allows spatially resolved, rather than line-of-sight, measurement. The application of elastic scattering depends strongly on the size of the particle. Complex Mie-scatter theory is required for particles and droplets, while a simpler Rayleigh-scatter assumption can be applied to small particles and molecules.

2.4.1 Mie Scatter

Gustav Mie developed an analytical solution to describe the scattering of light by spherical particles or droplets, given the light wavelength, the droplet diameter, and refractive index. Figure 8 shows the angular scattering intensity calculated from Mie's solution for a n-dodecane droplet with a diameter of 5 μm, a size that is typical for engine fuel sprays. The plot at the left indicates that the strongest scatter (by a factor of 10 or more) occurs in the forward direction (0°), but some light is also scattered sideward and backward. Scattering peaks and valleys (or lobes) also exist at discrete angles, for example near 30°, and these angles vary with droplet diameter.

The total scatter is also very sensitive to droplet diameter. The right of Figure 8 shows the extinction cross section σ_{ext} versus droplet diameter d, where σ_{ext} is proportional to the summation of light lost through the scattering process at all angles. Larger droplets more typical of a spray exhibit a d^2 dependency upon σ_{ext}, while small droplets and particles with diameters approximately less than the light wavelength fall into the Rayleigh-scatter regime and exhibit a d^6 dependency, as well as a simpler angular scattering pattern.

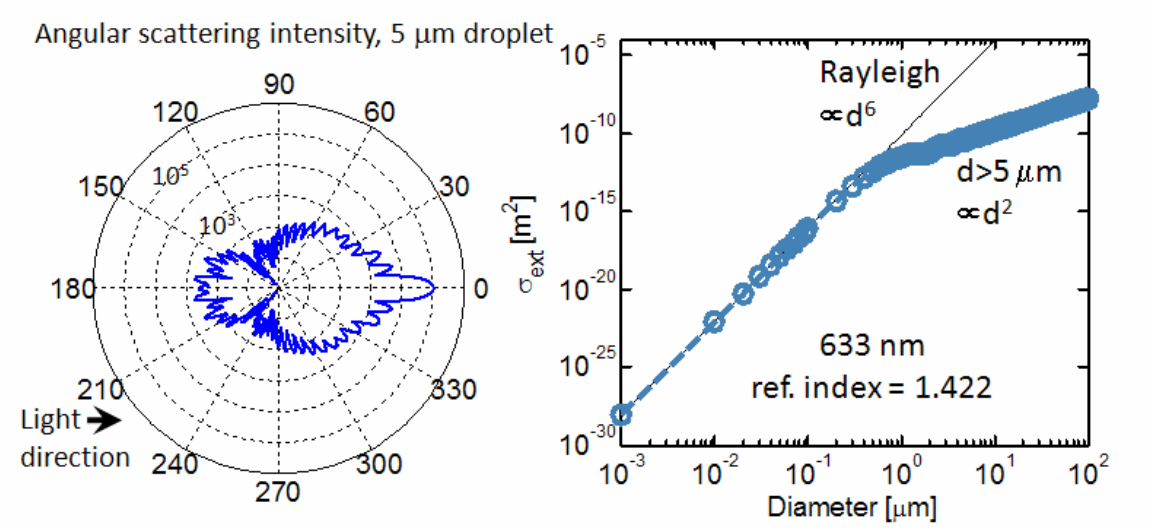

Figure 8. (left) Angular scattering intensity distribution (logarithmic scale) for a 5 µm n-dodecane droplet in air. (right) Extinction cross section as function of droplet diameter (logarithmic scale). Wavelength is 633 nm and unpolarized; droplet refractive index is 1.422.

Because of the difficulties associated with understanding the exact droplet diameter and collection angle, as well as the actual incident intensity after attenuation and scatter by other droplets, Mie scatter is typically not used to quantify total droplet concentration in engine applications. However, it can be used to identify if droplets do or do not exist at a particular location, and is therefore widely used for imaging in engines. In addition, Mie-scatter optical techniques, such as phase-Doppler interferometry, capitalize on the existence of angular scattering lobes indicated in Figure 8 as means for measuring droplet diameter size distributions within sprays [32].

2.4.2 Rayleigh Scatter

Elastic scatter from small, nanometer-sized particles exhibits Rayleigh-scattering behavior when using typical light sources. Soot particles or even gaseous fuel molecules fall into this regime. For example, the molecular size of vaporized n-dodecane is less than 2 nm and the extinction cross section $\sigma_{ext} = 8.5 \cdot 10^{-29}$ m^2 [33], consistent with the relationships shown in Figure 8. By comparison, σ_{ext} for a typical droplet is more than 15 orders of magnitude higher. This major difference effectively means that Rayleigh-scattering measurements must be performed in an environment without droplets or larger particles, and other scattering sources such as windows reflections must be minimized. If this can be achieved, Rayleigh-scattering offers the potential for quantitative measurement because, unlike droplet Mie-scattering, the scattering cross sections for gaseous fuel and oxidizer molecules are known [34].

Figure 9 shows a composite of a Mie scattering image (left) and a Rayleigh scattering image (top right) acquired in a vaporizing n-heptane fuel spray. The Mie scatter and Rayleigh scatter images are shown as a composite, but they were actually obtained at different instances with different experimental setups. The Mie scattering image shows that as the spray entrains and mixes with the hot ambient, all of the liquid fuel is eventually vaporized downstream of about 10 mm. A laser sheet positioned downstream

of this liquid droplet region induces Rayleigh scattering from fuel vapor and ambient gases without interference from liquid droplets.

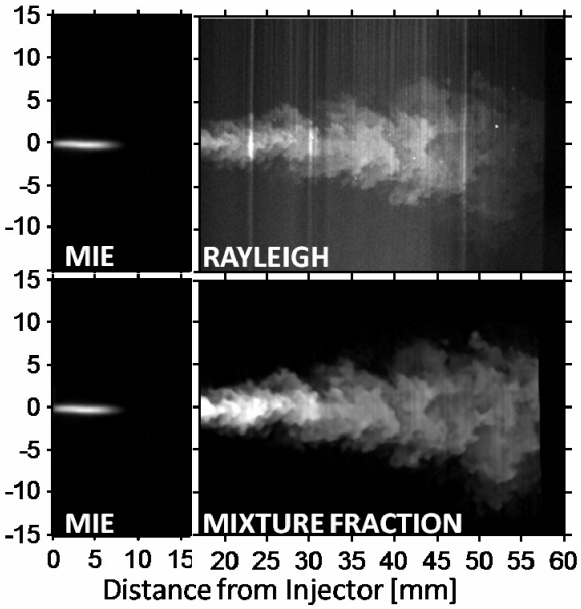

Figure 9. Composite image of Mie scattering (left) and Rayleigh scattering (right). Ambient conditions: 1000 K, 14.8 kg/m^3, 4.2 MPa, 0% O_2. Injector conditions: 0.100-mm orifice, 154 MPa, n-heptane. [33]

The Rayleigh scattering signature from the ambient gases outside of the spray creates reference data that permits corrections for laser sheet intensity variations caused by energy variation in the delivery beam as well as beam steering in the high-pressure combustion vessel. The laser energy variation is apparent in the raw Rayleigh image. Not only is the incoming laser intensity non-uniform, but as the laser beam propagates through the vaporized fuel spray from bottom to top there is additional beam refraction caused by temperature variation within the spray (see section 2.2 for more discussion on beam refraction). The success of these corrections is indicated by the fuel-ambient mixture fraction image at the bottom of the figure.

Further reading:

Espey, C., Dec, J.E., Litzinger, T.A., and Santavicca, D.A., "Planar laser Rayleigh scattering for quantitative vapor-fuel imaging in a diesel jet," Combustion and Flame 109:65-86, 1997.

2.5 Fluorescence

Like chemiluminescence (section 2.1.1), fluorescence refers to light emitted when an electronically excited molecule spontaneously transitions to a lower energy state. For fluorescence, the molecule is excited not by chemical reaction, but by absorption of light photon(s), typically from a laser source (laser-induced fluorescence, LIF). The photon absorption is typically very strong so combustion intermediate species can be detected down to ppm-level concentrations. As described in section 2.1.1, each molecular species

only absorb photons at specific wavelengths (colors), so specific species may be targeted if the available laser output wavelengths can be matched to the absorption wavelength of the target species. In combustion, many of the practically useful absorption lines are in the ultraviolet (UV) wavelength region.

After excitation into a specific energy state, various energy transfer processes (e.g., collisions) populate other rotational, vibrational, and even electronic states, typically with lower energy than the directly excited state. When these lower energy states transition back to the ground state, the emitted photon has less energy than the original excitation photon. Spectrally, this means the fluorescence emission occurs at a longer wavelength than excitation. This red-shift is of great practical importance, because it allows *blocking* the incident laser wavelength by suitable color-selective filters while still *detecting* the fluorescence signal. Thus the detector sees only the red-shifted fluorescence signal, not unwanted reflections and scattering of the laser-light at the unshifted color off windows, particles, etc.

Not all excited molecules emit a fluorescence photon. Collisions with other molecules can de-excite the excited molecule without emission of a photon, a process called *quenching*. The likelihood of quenching depends on pressure, temperature, and the collisional partner, that is, on the gas composition. There are also other non-collision de-excitation mechanisms, such as intersystem crossing and internal conversion, which depend on temperature. The overall likelihood of absorbing light and then returning to the ground state via fluorescence, or equivalently, the fraction of excitation photons that yield fluorescence photons, is called *quantum efficiency*.

As a result of the multitude of energy pathways in the fluorescence process, determination of the quantum efficiency requires knowledge of both the photophysical properties and the thermochemical environment of the molecule to be detected. The former is often not available from the literature for high temperature and pressure, the latter may not be known in combustion. Hence, quantification of fluorescence signals to determine concentration can be challenging or even impossible. On the other hand, these dependencies can sometimes be exploited to gain additional knowledge about the local temperature or gas composition. For these reasons, advancement of fluorescence measurements in engines crucially depends on improving our understanding of photophysics at engine-relevant conditions via fundamental experiments in pressurized, heated cells and shock tubes.

Further reading:

Eckbreth, A.C., *Laser diagnostics for combustion temperature and species*, Gordon and Breach, 1996.

2.5.1 Combustion Intermediates

Among the educts and products of complete combustion, neither nitrogen, oxygen, water, nor carbon dioxide can be detected by fluorescence in engines in a practically useful manner. However, some important combustion intermediates and fuel components have accessible electronic transitions making LIF a powerful tool for their in-cylinder measurement. Table 3 summarizes key features of fluorescence measurements in engines for five commonly detected combustion intermediates. All have fluorescence signals

strong enough for spatially resolved, two-dimensional planar laser-induced fluorescence (PLIF), although barely so in the case of CO. Note that, except for C_2, all excitation wavelengths are in the UV, which is typical for electronic absorption bands of small molecules.

Table 3: Qualitative overview of the most commonly used schemes for fluorescence measurements of combustion intermediates in engines. The excitation and detection wavelength given in column 2 and 3, respectively, are not the only possible choices. Like all other entries they merely represent the dominant literature values. Entries in parentheses represent less common choices.

Species	λ_{exc} [nm]	λ_{det} [nm]	Laser	Indicative for	Signal
OH	(248) 283	310	(KrF excimer) dye, OPO	high-T reactions	strong
H_2CO	353, 355	400 - 475	dye, Nd:YAG	low-T reactions	strong
NO	226 (248)	225 - 300	OPO (KrF excimer)	high T, pollutant	weak
CO	230	484	OPO	incomplete or rich combustion	very weak
C_2	355, 532	435 - 640	Nd:YAG	soot and its precursors	medium

The hydroxyl-radical (OH) is one of the most common targets for fluorescence measurements of combustion intermediates. Strong absorption features around 283.5 nm can be excited by use of tunable UV-lasers such as a frequency-doubled, Nd:YAG pumped dye laser or an optical parametric oscillator (OPO). In non-premixed combustion (classic Diesel), OH is formed in hot, stoichiometric or slightly fuel-lean mixtures. In premixed auto-ignition (HCCI), OH indicates the active second-stage ignition and the main phase of heat release. In premixed spark-ignition, the initial appearance of OH delineates the flame front, and it persists later in the burnt regions.

In addition to those listed in Table 3, many other species can be detected, though most of them not in the single-shot measurements that are necessary to “freeze” turbulent fluid motion. The main limitations are the lack of powerful, tunable, UV lasers that could utilize the weak transitions of the more “exotic” species and also interference of more common species.

Quantitative concentration measurements of combustion intermediates in engines are difficult and correspondingly uncommon. Major challenges are the lack of literature data on the species’ high-pressure, high-temperature photophysics, difficulties in calibrating against a known concentration (particularly for unstable intermediates), complicated dependencies of fluorescence on usually unknown local temperature and gas composition.

Fortunately, much can be learned from qualitative, spatially resolved measurements. Even more information can be extracted from combined measurements, for which LIF is very suitable, because often the signal is limited to a narrow spectral region and can be separated from other, simultaneously detected channels. For instance, consider the

images in Figure 10: We learn *where* OH is located in the spray flame, *when* it appears during the injection, and *where* it is in *relation* to the soot. From this we can infer that the edge of the spray flame is hot and stoichiometric to slightly fuel-lean, that this remains the case throughout the entire injection. Furthermore, OH and soot have very little spatial overlap, which indicates that the OH-containing edge is likely actively oxidizing soot.

Further reading: K. Kohse-Höinghaus, Prog. Energy Combust. Sci. 20 (3) (1994) 203-279 10.1016/0360-1285(94)90015-9.

2.5.2 Fuel and fuel-tracers

Most commercial fuels, with the notable exception of biodiesel, emit strong fluorescence when illuminated by UV lasers. Therefore LIF can used to detect both liquid and gas-phase fuel with good sensitivity. Two-dimensional, planar LIF (PLIF) is possible with several laser types, including excimer or Nd:YAG lasers. In some circumstances, conversion of the LIF signal to fuel concentration is possible, but in general quantification is difficult because commercial fuels are mixtures that contain multiple fluorescing components, many of which have unknown photophysical properties.

In quantitative LIF measurements, a non-fluorescing *model fuel* is typically doped with a *tracer*, which exhibits fluorescence with known characteristics. Ideally, the tracer behaves like the fuel in all physical and chemical aspects and the mixture of non-fluorescing model fuel and tracer behaves like the commercial fuel it is supposed to model. Conveniently, none of the aliphatic components in the traditional primary reference fuels for gasoline and diesel (n-heptane + iso-octane and n-cetane + iso-cetane, respectively) fluoresces significantly at near UV wavelengths. The most common types of tracers are one- or two-ring aromatics, ketones, aldehydes, and amines. The aromatic compounds also are also found in significant quantities in commercial fuels. Unlike the small combustion intermediate molecules with narrow absorption lines in Table 3, the larger tracer molecules have broad absorption spectra, covering tens of nanometers. Therefore, complicated and weak tunable lasers are usually not necessary. Tracer LIF is most often used to image the mixing of evaporated fuel and intake air, as for example shown in Article 10**.**

In engine applications, the photophysical processes of LIF are dependent on excitation wavelength, gas composition, pressure, and temperature. Each of these dependencies can be an obstacle in quantification of the measurements, but once known, can also give the opportunity to measure the quantity of influence. For example, the dependence of toluene fluorescence on temperature has been characterized in shock-tube and flow-cell experiments [35]. It can be exploited to determine that quantity based on either the red-shift of the emission spectrum with increasing temperature [36] or the overall decrease of signal with increasing temperature [37].

Two important limitations in the applicability of tracer LIF are the presence of liquid-phase fuel (spray) and the onset of combustion reactions. Fluorescence from a simultaneously present liquid phase is hard to quantify, although techniques exists to at least reliably separate it from gas-phase fluorescence (“Exciplex” fluorescence). The chemical reactions of combustion convert the tracer via usually unquantifiable intermediates into non-fluorescing species.

Further reading: C. Schulz; V. Sick, "Tracer-LIF diagnostics: quantitative measurement of fuel concentration, temperature, and fuel/air ratio in practical combustion systems," Prog. Energy Combust. Sci. 31 (1) (2005) 75-121 10.1016/j.pecs.2004.08.002.

2.6 Laser-Induced Incandescence of soot

As described in section 2.1.2, soot heated to high temperatures by combustion emits light by incandescence, and the intensity of the incandescence increases nonlinearly with temperature. For instance, according to equation (6), a 10% increase in temperature from 2400 K to 2500 K results in a 60% increase in light emission at 500 nm (green color). Using high-energy pulsed lasers, the soot particles can be heated by absorbing laser light to much higher temperatures. The laser-heating limit is the vaporization temperature of the soot, which is approximately 4000-4500 K. At 4000 K, the emission at 500 nm increases by a factor of 120 relative to 2400 K. As a result, laser-induced incandescence (LII) emission captured over the duration of the short (typically ~10 ns) high-power laser pulse can be dominated by the laser-heated soot.

In theory, the LII technique can be quantitative. The soot temperature should remain at a steady level during vaporization (akin to boiling water), so that the signal becomes independent of laser intensity. Hence, above the vaporization threshold intensity, the LII emission should be independent of the local laser intensity. At a constant temperature, the LII signal is approximately proportional to the soot volume fraction.

One advantage of the LII technique over other line-of-sight techniques like 2-color soot incandescence technique described in section 2.1.2 is that the laser-induced emission arises only from sooty regions that intersect with the path of the laser beam. Hence, laser-induced incandescence of soot can provide spatial resolution along the line-of-sight of the detector.

To achieve the laser-light intensities required to heat soot particles to their vaporization temperature, even high-power beams typically must be focused to a small region. For imaging techniques, the laser beam is focused into a thin sheet (1 mm thick or less) for planar laser-induced incandescence (PLII) of soot. Figure 10 shows a series of composite images of PLII of soot (red) with PLIF of OH (green) for one of eight diesel jets in an optical diesel engine [38].

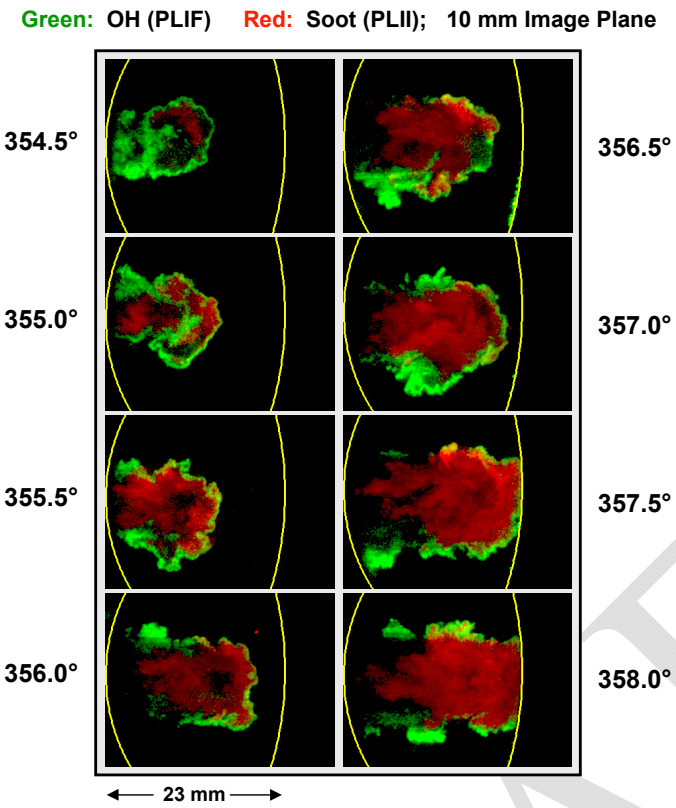

Figure 10. Series of simultaneous OH PLIF (green) and soot PLII (red) images [38]. The numbers beside the images indicate the crank angle of acquisition, with 360° at top-dead center. The yellow curve at the left marks the edge of a window in the cylinder head, and the curve at the right marks the piston bowl wall.

In addition to the images in Figure 10, a few other notable examples of soot LII measurements are: soot LII in a DI diesel engine [39], combined soot extinction and LII in a gasoline direct injection engine {de Francqueville, 2010 537 /id}, and high-speed soot LII in a lab burner and in an optical engine [40].

Although soot LII can be quantitative in principle, several factors introduce significant uncertainty. The vaporization-temperature signal-plateau predicted by theory is not observed in practice because of non-uniform laser beam intensity distributions and obliteration of soot particles by excessive vaporization at high laser-beam intensities. Interferences from other effects, including fluorescence of photolysis products like C_2 and C_3, as well as fluorescence of polycyclic aromatic hydrocarbon soot precursor species, can also spectrally and temporally overlap with the LII emission. Also, while the LII emission is much stronger than the combustion-heated soot emission within the measurement volume, integration of the combustion-heated soot along the whole line of sight from the detector can be a significant interference, depending on the soot cloud geometry.

Further Reading:

Santoro, R.J. and Shaddix, C.R. *Applied Combustion Diagnostics, Chapter 9: Laser-induced incandescence*, Kohse-Höinghaus, K. and Jeffries, J.B. Eds., Taylor and Francis, 2002.

Schulz, C., Kock, B.F., Hofmann, M. Michelsen, H., Will, S., Bougie, B., Suntz, R., and Smallwood, G. "Laser-induced incandescence: recent trends and current questions," Applied Physics B 83, 333-354, 2006.

2.7 Velocimetry

In-cylinder convection and turbulence are two flow properties of paramount importance to engine operation because they determine transport and mixing, discussed in detail in Article 11. Two families of diagnostics have been applied in engines to measure velocity: The two-dimensional techniques particle image velocimetry (PIV) and particle tracking velocimetry (PTV), and the point-measurement laser-Doppler velocimetry (LDV).

The velocity of spray droplets can be measured directly. On the other hand, in engines, gas-phase velocity almost always needs to be measured indirectly using small particles seeded into the intake gas. Seeding is far from trivial. Particles need to be

- Present at all measurement locations and timings in the right density, which is dependent on the technique
- Small enough to follow the flow with the required fidelity, but large enough to enough scatter light for reliable detection
- Not interfere with the measurement by fouling the windows or disturbing the flow itself
- Survive the high temperatures of compression or even combustion as required by the measurement timing

In fact, ongoing development aside, the diagnostics described below are fairly mature. The challenge in engines is proper seeding. Typical seed particles are droplets from liquids with high boiling point, like silicone oil or di-ethyl-hexyl-sebacate (DEHS), or (less commonly) solid particles from silicon dioxide, graphite, or hollow glass spheres. Liquid seeding does not survive combustion, which can also be an advantage, because the absence of seeding then approximately marks the burned gas.

For engines, particles with diameters on the order of 20 μm follow the mean bulk flow with sufficient fidelity, while investigating small-scale turbulence or highly rotational flows may require particles sizes of less than 1 μm. If quantitative results are the goal, a case-based comparison of the expected accelerations (i.e., particle inertia) and aerodynamic drag is required.

The development of velocimetry, particularly in the case of PIV, has greatly profited from the broad range of applications. Uniquely among the diagnostics discussed here, complete systems including lasers, detectors, as well as computer units for timing, data acquisition, and data evaluation are commercially available from several companies. This should not detract from the fact that reliable measurements in engines are still not easy.

2.7.1 PIV and PTV

Both PIV and PTV are based on the same principle: Particles in an extended probe volume, typically a plane of about 1 mm thickness, are illuminated by two (or more) laser pulses separated by known time interval(s). An image of the light scattering from the particles is acquired with each laser pulse. The measured particle displacement divided

by the inter-pulse time yields velocity vectors throughout the field of view. In the basic configuration, the two in-plane components of the velocity vector are determined, but extensions exist for capturing all three, and potentially not only in a plane, but within a volume. Extracting more information requires more cameras and better optical access, which limits the applicability in engines.

The difference between PIV and PTV is in the data evaluation, which corresponds to a difference in seeding density. In PTV, the seeding density is low, thus bright spots (i.e., particles) in the images are sparse. This allows for tracking the displacement of individual particles between the two images with little ambiguity. Each particle yields one velocity vector. In PIV, seeding is dense in the sense that the displacement of individual particles cannot be determined unambiguously. Instead, the image is partitioned into many "interrogation areas", each large enough to contain at least several particles. Via cross-correlation of two corresponding interrogation areas in the two images the average displacement within the area is calculated. Each velocity vector relies on data from all particles in the interrogation area, increasing precision. Also, PIV can achieve higher resolution when seeding is sufficiently dense. When dense seeding cannot be achieved, PTV is advantageous. Hybrid techniques for spatially very inhomogeneous seeding exist. Figure XXX in Article 11 shows examples of flow fields acquired by PIV.

Further reading: M. Raffel; C. Willert; S. Wereley; J. Kompenhans, Particle Image Velocimetry: A Practical Guide, Springer, New York, 2007

2.7.2 LDV and PDA

While PIV and PTV provide instantaneous measurements across an extended field of view, LDV delivers a nearly continuous stream of velocity data from particles passing through a small, point-like probe volume. In LDV, also called laser Doppler anemometry (LDA), two coherent laser beams of the same (or very nearly the same) wavelength are focused into the probe volume at a small angle such that an interference pattern is formed. Particles moving through this spatial intensity modulation cause temporally varying scattering, which is detected by receiving optics. The transverse component of the particle velocity can be determined from the modulation frequency. Each passing particle yields one data point. The data rate depends on flow velocity and seeding density, but rates of tens of kilohertz are achievable. Extensions with multiple lasers and detectors can measure more than one vector component.

Another important extension of LDV is phase Doppler anemometry, PDA, applicable to transparent particles such as droplets from a spray [32]. In this technique a suitably located second receiver allows for determination of droplet size in addition to velocity. PDA is a powerful tool for the quantitative study of injection sprays and as such is indispensable for the development of computational spray models.

Reference List

1. Dec, J. E., Hwang, W., and Sjöberg, M., "An investigation of thermal stratification in HCCI engines using chemiluminescence imaging," SAE Paper 2006-01-1518, SAE Trans. 115(3):759-776 (2006).

2. Bowditch, F. W., "A new tool for combustion research: a quartz piston engine," SAE Paper 610002, SAE Trans. 69:17-23 (1961).

3. Kashdan, J. T. and Thirouard, B., "A comparison of combustion and emissions vehaviour in optical and metal single-cylinder diesel engines," SAE Paper 2009-01-1963, SAE Int.J.Engines 2:1857-1872 (2009).

4. Aronsson, U., Chartier, C., Horn, U., Anderson, Ö, Johansson, B., and Egnell, R., "Heat release comparison between optical and all-metal HSDI diesel engines," SAE Paper 2008-01-1062, (2008).

5. Aronsson, U., Solaka, H., Chartier, C., Andersson, Ö, and Johansson, B., "Impact of mechanical deformation due to pressure, mass, and thermal forces on the in-cylinder volume trace in optical engines of Bowditch design," SAE Paper 2011-26-0082, (2011).

6. Colban, W., Kim, D., Miles, P. C., Oh, S., Opat, R., Krieger, R., Foster, D., Durret, R. P., and Gonzalez D.M.A., "A detailed comparison of emissions and combustion performance between optical and metal single-cylinder diesel engines at low temperature combustion conditions," SAE Paper 2008-01-1066, SAE Trans. 117(4):505-519 (2008).

7. Donovan, M. T., He, X., Zigler, B. T., Palmer, T. R., Wooldridge, M. S., and Atreya, A., "Demonstration of a free-piston rapid compression facility for the study of high temperature combustion phenomena," Combust.Flame 137:351-365 (2004).

8. Watanabe, Y., Morikawa, K., Kuwahara, T., and Tanabe, M., "Evaluation of homogeneous charge compression ignition at high engine speeds using a super rapid compression machine," SAE Paper 2008-01-2403, (2008).

9. Siebers, D. L. and Higgins, B. S., "Flame lift-off on direct-injection diesel sprays under quiescent conditions," SAE Paper 2001-01-0530, SAE Transactions 110(3):400-421 (2001).

10. Oren, D. C., Wahiduzzaman, S., and Ferguson, C. R., "A diesel combustion bomb: proof of concept," SAE Paper 841358, (1984).

11. Ikeda, Y., Kaneko, M., and Nakajima, T., "Local A/F measurement by chemiluminescence of OH*, CH* and C2* in SI engine," SAE Paper 2001-01-0919, (2001).

12. Augusta, R., Foster, D. E., Ghandhi, J. B., Eng, J., and Najt, P. M., "Chemiluminescence measurements of homogeneous charge compression ignition (HCCI) combustion," SAE Paper 2006-01-1520, (2006).

13. Kokjohn, S., Musculus, M. P. B., and Reitz, R. D., "Investigation of fuel reactivity stratification for controlling PCI heat-release rates using high-speed

chemiluminescence imaging and fuel tracer fluorescence," SAE Paper 2012-01-0375, (2012).

14. Svensson, K. I., Mackrory, A. J., Richards, M. J., and Tree, D. R., "Calibration of an RGB, CCD camera and interpretation of its two-color images from KL and temperature," SAE Paper 2005-01-0648, (2005).

15. Mueller, C. J. and Martin, G. C., "Effects of oxygenated compounds on combustion and soot evolution in a DI diesel engine: broadband natural luminosity imaging," SAE Paper 2002-01-1631, SAE Transactions 111(4):518-527 (2002).

16. Pastor, J. V., Garcia, JM, Pastor, J. M., and Buitrago, J. E., "Analysis methodology of diesel combustion by using flame luminosity, two-color method, and laser-induced incandescence," SAE Paper 2005-24-012, (2005).

17. Musculus, M. P. B., Singh, S., and Reitz, R. D., "Gradient effect on two-color soot optical pyrometry in a heavy-duty DI diesel engine," Combust.Flame 153(1-2):216-227 (2008).

18. Birkigt, A., Michels, K., Theobald, J., Seeger, T., Gao, Y., Weikl, M. C., Wensing, M., and Leipertz, A., "Investigation of compression temperature in highly charged spark-ignition engines," Int.J.Engine Res. 12(3):282-292 (2011).

19. Settles, G. S., *Schlieren and shadowgraph techniques*, Springer-Verlag (2001).

20. Pickett, L. M., Kook, S., and Williams, T. C., "Visualization of diesel spray penetration, cool-flame, ignition, high-temperature combustion, and soot formation using high-speed imaging," SAE Paper 2009-01-0658, SAE Int.J.Engines 2(1):439-459 (2009).

21. Naber, J. D. and Siebers, D. L., "Effects of gas density and vaporization on penetration and dispersion of diesel sprays," SAE Paper 960034, SAE Transactions 105(3):82-111 (1996).

22. Pawlowski, A., Kneer, R., Lippert, A., and Parrish, S. E., "Investigation of the interaction of sprays from clustered orifices under ambient conditions relevant for diesel engines," SAE Paper 2008-01-0928, SAE Trans. 514(4):514-527 (2008).

23. Idicheria, C. A. and Pickett, L. M., "Soot formation in diesel combustion under high-EGR conditions," SAE Paper 2005-01-3834, SAE Transactions 114(4):1559-1574 (2005).

24. de Francqueville, L., Bruneaux, G., and Thirouard, B., "Soot volume fraction measurements in a gasoline direct injection engine by combined laser induece incandescence and laser extinction method," SAE Paper 2010-01-0346, SAE Int.J.Engines 3:163-182 (2010).

25. Williams, T. C., Shaddix, C. R., Jensen, K. A., and Suo-Anttila, J. M., "Measurement of the dimensionless extinction coefficient of soot within laminar diffusion flames," Int.J.Heat Mass Trans. 50(7-8):1616-1630 (2007).

26. Xu, Y. and Lee, C., "Investigation of fuel effects on soot fomration using forward illumination light extinction (FILE) technique," SAE Paper 2005-01-0365, (2005).

27. Ghandhi, J. B. and Heim, D. M., "An optimized optical system for backlit imaging," Review of Scientific Instruments 80(5):056105 (2009).

28. "Gasoline fuel injector spray measurement and characterization," SAE Standard J2715 (2007).

29. Berrocal, E., Kristensson, E., Richter, M., Linne, M., and Aldén, M., "Application of structured illumination for multiple scattering suppression in planar laser imaging of dense sprays," Optics Express 16:17870-17881 (2008).

30. Linne, M. A., Paciaroni, M., Berrocal, E., and Sedarski, D., "Ballistic imaging of liquid breakup processes in dense sprays," Proc.Combust.Inst. 32:2147-2161 (2009).

31. Kastengren, A. L., Powell, C. F., Wang, Y. J., Im, K. S., and Wang, J., "X-Ray radiography measurements of diesel spray structure at engine-like ambient density," Atomization and Sprays 19:1031-1044 (2009).

32. Sankar, S. V., Weber, B. J., Kamemoto, D. Y., and Bachalo, W. D., "Sizing fine particles with the phase Doppler interferometric technique," Appl.Opt. 30:4914-4920 (1991).

33. Pickett, L. M., Manin, J., Genzale, C. L., Siebers, D. L., Musculus, M. P. B., and Idicheria, C. A., "Relationship between diesel fuel-jet vapor penetration/dispersion and local fuel mixture-fraction," SAE Paper 2011-01-0686, (2011).

34. Idicheria, C. A. and Pickett, L. M., "Quantitative mixing measurements in a vaporizing diesel spray by Rayleigh imaging," SAE Paper 2007-01-0647, SAE Transactions 116 (2007).

35. Koban, W., Koch, J. D., Hanson, R. K., and Schulz, C., "Absorption and fluorescence of toluene vapor at elevated temperatures," Phys.Chem.Chem.Phys. 6:2940-2945 (2004).

36. Luong, M., Zhang, R., Schulz, C., and Sick, V., "Toluene laser-induced fluorescence for in-cylinder temperature imaging in internal combustion engines," Appl.Phys.B-Lasers Opt. 91(3-4):669-675 (2008).

37. Dec, J. E. and Hwang, W., "Characterizing the development of thermal stratification in an HCCI engine using planar-imaging thermometry," SAE Paper 2009-01-0650, SAE Int.J.Engines 2:421-438 (2009).

38. Dec, J. E. and Tree, D. R., "Diffusion-flame / wall interactions in a heavy-duty DI diesel engine," SAE Paper 2001-01-1295, SAE Transactions 110(3):1618-1634 (2001).

39. Pinson, J. A., Mitchell, D. L., Santoro, R. J., and Litzinger, T. A., "Quantitative, planar soot measurements in a D.I. diesel engine using laser-induced incandescence and light scattering," SAE Paper 932650, (1993).

40. Sjöholm, J., Wellander, R., Bladh, H., Richter, M., Bengtsson, P. E., Aldén, M., Aronsson, U., Chartier, C., Andersson, Ö, and Johansson, B., "Challenges of in-cylinder high-speed two-dimensional laser-induced incandescence measurements of soot," SAE Paper 2011-01-1280, SAE Int.J.Engines 4(1):1607-1622 (2011).